Int. J. Electrochem. Sci., 14 **(2019)** 10582 – 10591, doi: 10.20965/2019.11.53

International Journal of
ELECTROCHEMICAL
SCIENCE
www.electrochemsci.org

Synthesis and Electrochemical Properties of $Fe_{1-x}S$@C with Good Stability as an Anode Material for Lithium Ion Batteries

Yimeng Liao, Yanhui Zhang, Zhi Su[*]*, Hualing Tian*

College of Chemistry and Chemical Engineering, Xinjiang Normal University, Urumqi, 830054 Xinjiang, China
[*]E-mail: suzhixj@sina.com

Received: 28 March 2019 / *Accepted:* 4 May 2019 / *Published:* 7 October 2019

In this study, we use a rapid, convenient, and cost-effective precipitation method to synthesis $Fe_{1-x}S$@C anode materials for use in lithium ion batteries (LIBs). We found that using a special carbon source acetylene black can lead to higher discharge specific capacity and a long cycling life of the LIB with $Fe_{1-x}S$@C anode. The sample prepared with 10 wt% of the carbon source and calcined at 600 °C showed the best electrochemical performance. The optimum $Fe_{1-x}S$@C sample maintained a very stable state after the initial 30 cycles of attenuation at 100 $mA \cdot g^{-1}$ and exhibited a high and stable reversible capacity of 644 $mA \cdot h \cdot g^{-1}$ until the 200th cycle.

Keywords: lithium-ion battery; anode material; $Fe_{1-x}S$@C; precipitation method; Electrochemical properties

1. INTRODUCTION

The current rapid development of various technologies has increased the demand for energy, which necessitates that energy storage equipment keep pace with such demands. In particular, the emergence and gradual popularization of new energy vehicles has led to the continuous development of battery technologies. Lithium-ion batteries (LIBs) are the most widely used secondary batteries at present, are also being constantly developed and improved [1-3]. Although research on alternative batteries with low cost and highly abundant elements has continued, there are still many unresolved difficulties remain so that research on such batteries is still in the laboratory stage and cannot be commercialized yet [4-6]. Therefore, LIBs are still likely to be the best choice for large-scale power batteries for a long time in the future, and research toward improving the performance of LIBs will continue [7-9].

Electrode materials are the most important component of LIBs that determine the performance of the batteries. While the traditional anode material, graphite, cannot keep up with the demand of the next-generation high-performance LIBs, the development of the next generation of high-performance electrode materials with long cycle stability, and high capacity has become the primary task of researchers at this stage [10,11]. For example, Tarascon [12] first reported the transition metal oxides as the anode materials of LIBs. In 2000, transition metal sulfides also began to attract the attention of researchers [13]. Similar to the properties of transition metal oxides, transition metal sulfides also have a high theoretical capacity, and the transition metal sulfide has better reversible capacity than the transition metal oxide. Among these, iron sulfide has a high theoretical capacity and Fe is an abundant element. Such compounds can not only undergo redox reactions with lithium ions, but their S-Fe-S layered structure also enables lithium ion intercalation into the van der Waals gaps, and thus, researchers believe that this kind of material have good application prospects [14-16]. Iron sulfide also has critical shortcomings. Their poor conductivity and structural collapse caused by large volume changes that lead to poor cycle stability are some of the issues to be overcome [17,18]. Common methods for improving the properties of iron sulfide mainly include, introducing a suitable carbon source, designing reasonable nanostructure forms of the material, or compounding it with other materials. Researchers usually use one or more of these methods to improve the electrochemical properties of the material [19-21]. Zhu et al. successfully combined porous electrospinning technology with a biomolecule-assisted hydrothermal method to prepare porous graphite carbon nanowires containing FeS nanodots [22]. The anode material showed relatively good performance in LIBs, a satisfactory discharge capacity of 400 $mA \cdot h \cdot g^{-1}$ has been achieved at a test conditions of 0.5C. Pan et al. prepared $Fe_3O_4/Fe_{1-x}S@C@MoS_2$ nanosheets in two steps using freeze-drying and hydrothermal methods [23]. The anode material exhibits wonderful charge/discharge performance and superior cycle performance whether used in SIBs (sodium ion batteries) or LIBs. When used in LIBs and selecting a rate of 200 $mA \cdot g^{-1}$, an amazing reversible capacity exceeds 1000 $mA \cdot h \cdot g^{-1}$.

However, most of these methods are complicated with the synthetic steps being cumbersome, the output of the product is limited, and the morphology and uniformity of the nanostructures are difficult to control, all of which are the reasons why this material is difficult to commercialize. In this study, we selected acetylene black as a carbon source, used a fast, low-cost, convenient, and high-yield precipitation method to prepare $Fe_{1-x}S@C$ anode materials for lithium-ion batteries. The resulting product performs surprisingly well as an anode. The results show that the synthesized material has superior electrochemical properties.

2. EXPERIMENTAL

The chemical reagents were used directly after purchase and without any purification. First, an appropriate amount of acetylene black (ACET) was taken in a beaker, and 50 mL of deionized water and an appropriate amount of polyvinylpyrrolidone were added and the mixture was sonicated for 1 h. Then, mixed 5.4058 g of $FeCl_3 \cdot 6H_2O$ with 3.0448 g of CN_2H_4S into a beaker, added 100mL of deionized water to obtain a homogeneous solution. The ultrasonically dispersed acetylene black

suspension was directly added to this mixed solution and stirred at room temperature for 12 h. Subsequently, the mixture was transferred to an evaporating dish and placed in a blast drying oven for 24 h at 80 °C, the precursor was obtained. Thereafter, the obtained precursor was placed in a tube furnace and calcined at 500, 600, and 700 °C for 4 h under argon. The obtained black powders were washed thrice with deionized water and thrice with absolute ethanol, and then placed in a blast drying oven at 80 °C until they dried completely.

X-ray diffraction (XRD, Bruker D2 diffractometer, using Cu *Kα* radiation source, λ = 1.5408 Å) was used to probe the phase composition of $Fe_{1-x}S$@C. The structure and size of $Fe_{1-x}S$@C were characterized by transmission electron microscopy (TEM, JEN-2010-FEE). The obtained materials were mixed with PVDF at a mass ratio of 1:1 and form a slurry by added deionized water of 2–3 ml. Then, selected smooth flat copper foil as the current collector, uniformly coated the slurry to obtain the $Fe_{1-x}S$@C anode, which was then dried at 70 °C for 10 h. A button battery was assembled in a hand-operated box. A solution of $LiPF_6$ (the volume ratio of dimethyl carbonate: ethylene carbonate: ethyl methyl carbonate = 1:1:1) as an electrolyte, at the same time Li metal as the counter electrode. After stood for 12 h, the electrochemical performance of the assembled battery was allowed to evaluate. Constant current charge /discharge and cycle life tests were carried out by a LAND-CT2001A battery test system (voltage range~0.01 to 3 V). Cyclic voltammetry (CV, scan rate~0.0005 $mV \cdot s^{-1}$, voltage range~0.01 to 3 V) and AC impedance (voltage range~0.01 to 3 V, frequencies ranging~0.01 Hz to 0.1 MHz) measurements were both tested on an electrochemical workstation (CHI-650D Shanghai Chenghua of China).

3. RESULTS AND DISCUSSION

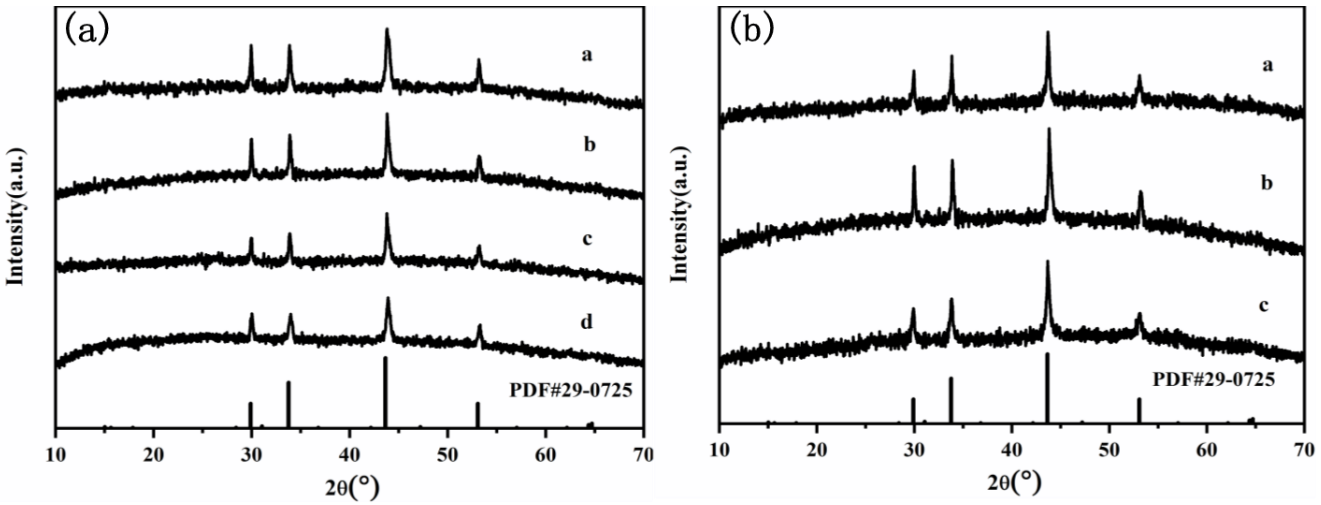

Figure 1. (a) XRD pattern of $Fe_{1-x}S$ @C with different amounts of acetylene black at 600 °C (a, b, c and d represent the carbon coating of 0, 5, 10 and 15 wt%, respectively); (b) XRD pattern of $Fe_{1-x}S$@C with 10 wt% ACET at different calcination temperature (a, b, and c represent the calcination temperature of 500, 600 and 700 °C, respectively).

Figure 1 exhibits the XRD diffraction diagram obtained under different experimental conditions. Fig.1. (a) shows patterns of $Fe_{1-x}S$ @C with different amounts of acetylene black at a calcination temperature of 600 °C, the letters a, b, c and d marked in the figure represent the carbon coating amount of 0, 5, 10, 15 wt%, respectively. Fig.1. (b) shows patterns of $Fe_{1-x}S$@C with 10 wt% ACET at different calcination temperature, the letters a, b, and c marked in the figure represent the calcination temperature of 500, 600 and 700 ℃, respectively. All XRD diffraction peaks of the prepared samples are consistent with hexagonal $Fe_{1-x}S$ (JCPDS card #29-0725) [6,24], indicating that the prepared samples are all $Fe_{1-x}S$@C materials. The sharp peak shapes of the samples indicate the high degree of crystallinity . The carbon coated on the material is in an amorphous state, which is proved by the fact that no distinct diffraction peak of carbon is observed in the figure.

Figure 2 shows the morphology of the $Fe_{1-x}S$@C material. The TEM exhibits a random block shape, with the dark portion in the TEM image being $Fe_{1-x}S$ and the lighter portion at the periphery being carbon coated on the surface of the sample in an amorphous form. These carbon wrapped on the surface can not only serve as a substrate for conduction during electron transfer but also enhance the stability of the material structure during the electrochemical reaction, thereby greatly improving the electrochemical performance of the samples [25,26]. The interplanar spacing of the material corresponding to the (200) crystalline plane of the $Fe_{1-x}S$ material can also be observed in Figure 2, and the calculated numerical result is ~ 0.31 nm. The result of the TEM analysis are mutually demonstrated with the XRD results we obtained earlier.

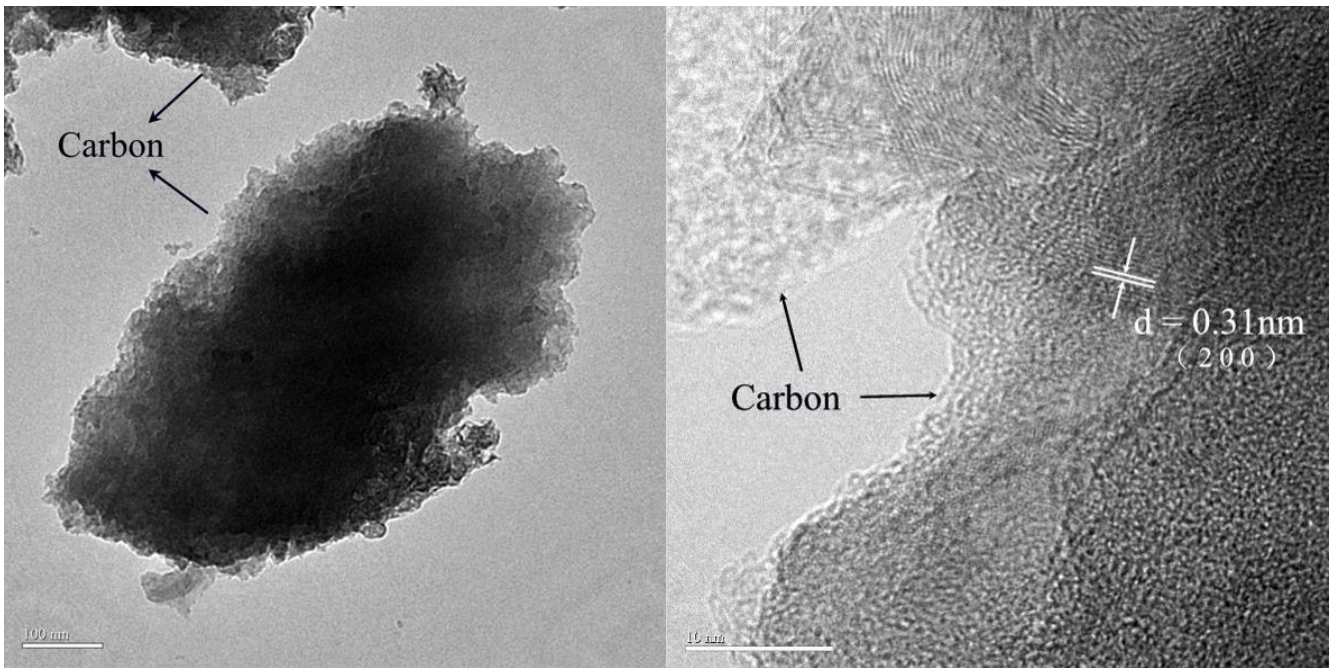

Figure 2. TEM image of $Fe_{1-x}S$@C materials

Figure 3(a) and Figure 3(b) shows the first cycle charge and discharge curves and the cycle life diagrams of $Fe_{1-x}S$@C coated with different amounts of ACET at 600 °C, respectively. The letters a, b,

c and d represent the ACET amount of 0, 5, 10, 15 wt%, respectively. With the performance curve comparison of $Fe_{1-x}S$@C and pure $Fe_{1-x}S$, we can conclude that the carbon coating is an effective modification method which can significantly improve the electrochemical performance of the sample. The thin carbon layer can buffer the structural collapse and large volume changes caused by the process of insertion/ extraction of lithium ion. In addition, carbon coating can also enhance the electronic conductivity and Li storage of our prepared samples. Using acetylene black as the carbon source results in a relatively high first-cycle discharge specific capacity, but the first-cycle charging specific capacity is far less than this high value, resulting the Coulomb efficiency of the first cycle was not ideal, but the discharge specific capacity and cycle stability are excellent.

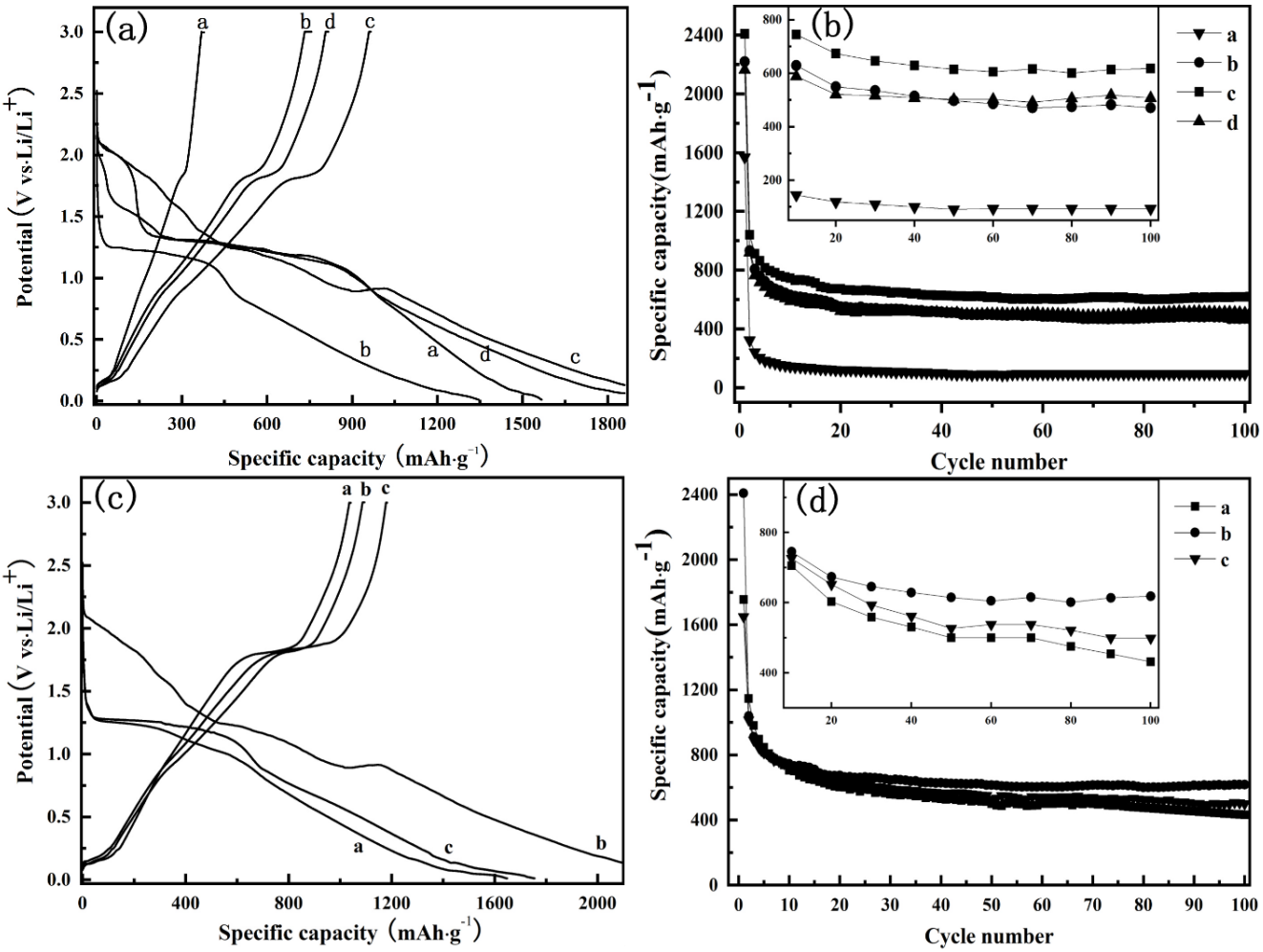

Figure 3. (a) First cycle charge and discharge profiles of $Fe_{1-x}S$@C coated with different amounts of acetylene black at 600 °C (a, b, c and d represent the carbon coating of 0, 5, 10 and 15 wt%, respectively); (b) Cycle life of $Fe_{1-x}S$@C coated with different amounts of acetylene black at 600 °C (a, b, c and d represent the carbon coating of 0, 5, 10 and 15 wt%, respectively); (c) First cycle charge and discharge profiles of $Fe_{1-x}S$@C (10 wt% ACET) at different calcination temperatures (a, b, and c represent the calcination temperature of 500, 600 and 700 ℃, respectively); (d) Cycle life of $Fe_{1-x}S$@C (10 wt% ACET) at different calcination temperature (a, b, and c represent the calcination temperature of 500, 600 and 700 ℃, respectively).

With increasing amount of ACET, the discharge specific capacity of the material increases first, reaches a maximum at 10 wt% and then begins to decrease. When the amount of carbon coating increase to 15 wt%, the reversible capacity of the material is reduced, which possibly due to the excessively high content of carbon reduces the tap density of the material or exacerbates the agglomeration of the material particles. Therefore, 10 wt% is the optimum coating amount of ACET. Figure 3(c) and Figure 3(d) are the cycle life diagrams and the first week charge and discharge curves of $Fe_{1-x}S$@C (10 wt% ACET) at different calcination temperatures, respectively. The letters a, b, and c represent the calcination temperatures of 500, 600 and 700 ℃, respectively. The calcination temperature has a very significant effect on the electrochemical performance of the sample, in agreement with the previously reported literature [6]. It can be seen that appropriately increase the calcination temperature can improve electrochemical performance of the material, but Coulomb efficiency of the first cycle does not have a good and regular effect. When the calcination temperature is insufficient, the crystal does not grow completely. Thereafter, as the calcination temperature increases, the particles of the material become larger and the agglomeration is aggravated, making the performance of the material unsatisfactory. In conclusion, the most suitable calcination temperature is 600 ℃. In summary, optimum results were obtained when 10 wt% ACET was used for carbon coating in the synthesis and the material was calcined at 600 °C. The samples prepared under such conditions exhibited the best electrochemical performance, including the most stable long cycle performance and the highest reversible capacity.

Figure 4 shows a long cycle life diagram of the material under the optimal condition at 100 $mA \cdot g^{-1}$. In the first few cycles, it can be observed that the discharge curve has a very significant drop. This irreversible loss of capacity should be mainly caused by structural collapse and the formation of the solid-electrolyte interface (SEI) film [23-25]. It tends to be stable while the 30th cycle. The optimum $Fe_{1-x}S$@C sample exhibits a pretty good reversible capacity of 644 $mA \cdot h \cdot g^{-1}$ until the 200th cycle, and the curve is very smooth while it maintains a very stable trend.

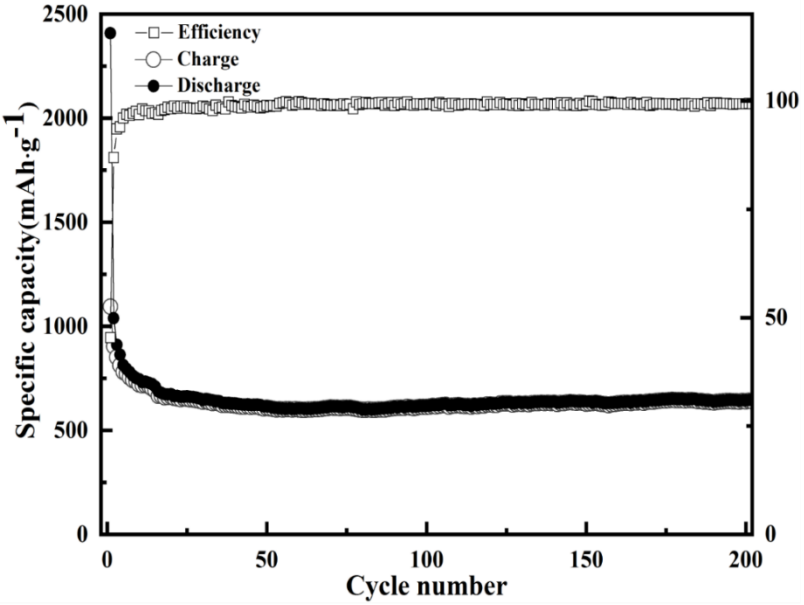

Figure 4. The cycle performance of $Fe_{1-x}S$@C with 10 wt% ACET at 600 ℃.

Figure 5 shows the cycle performance profiles of $Fe_{1-x}S$@C (10 wt% ACET, 600 ℃) at different rates. The initial test rate is 100 $mA \cdot g^{-1}$, and the numerical value increases by 100 every 10 cycles until up to 500 $mA \cdot g^{-1}$, and then continues to cycle at 100 $mA \cdot g^{-1}$. The discharge curve of the material shows a large attenuation in the first 10 cycles then tends to be stable. The electrode delivers 560, 510, 490, and 470 $mA \cdot h \cdot g^{-1}$ capacity at 200, 300, 400, and 500 $mA \cdot g^{-1}$, respectively, with satisfactory stability. In the 50th cycle, the current density was reverted to 100 $mA \cdot g^{-1}$, the discharge specific capacity of the material remained at 640 $mA \cdot h \cdot g^{-1}$ after a small attenuation, indicating the wonderful cycle stability of the sample. The results of these electrochemical properties of $Fe_{1-x}S$ based materials are very prominent in the reported literature. (Table 1)

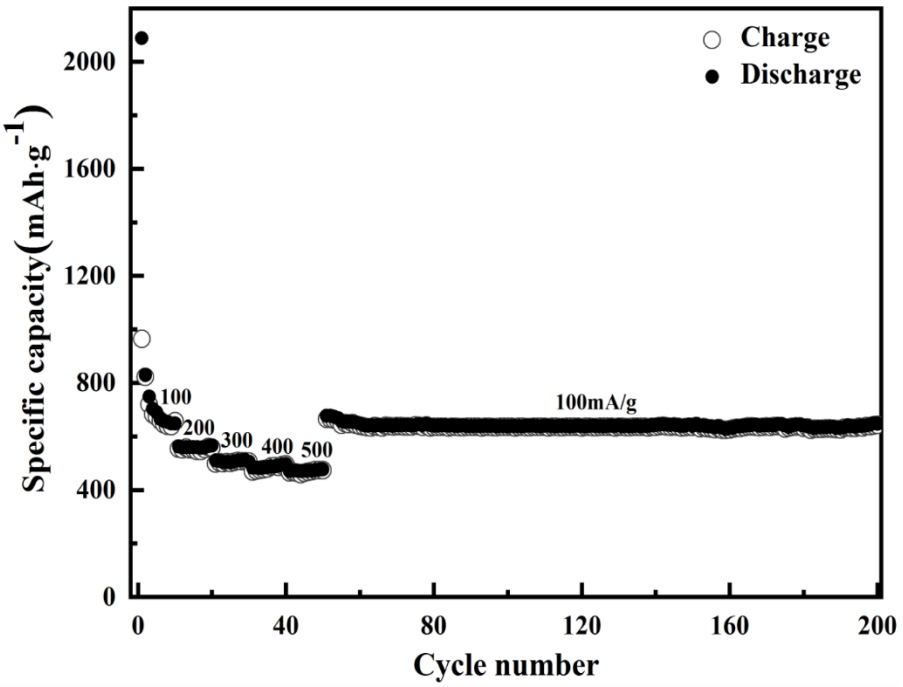

Figure 5. Charge and discharge profiles of $Fe_{1-x}S$@C with 10 wt% ACET at 600 ℃ at different rates.

Table1: Comparison of electrochemical performance of $Fe_{1-x}S$ ($x \geqslant 0$) materials (this paper and previous reported data).

Author	Material	discharge capacity ($mA \cdot h \cdot g^{-1}$)	Cycle number	current density ($mA \cdot g^{-1}$)
X. Wei et al. [17]	FeS	420	100	91
		395	15	457
C. Zhu et al. [22]	FeS	400	50	305
		458	10	609
Z. Yan et al. [26]	$Fe_{1-x}S$	632	200	100
		395	20	500
Sample of this work	$Fe_{1-x}S$	644	200	100
		470	50	500

As shown in Table 1, we compared the electrochemical properties of the prepared sample with similar anode materials for LIBs that were described in literature. It can be clearly observed that at approximate current density, the sample we prepared has a higher reversible capacity and excellent cycle stability. In addition, the sample also has satisfactory rate performance. The reversible capacity and stability of the sample at high rate are better than those reported in the literature.

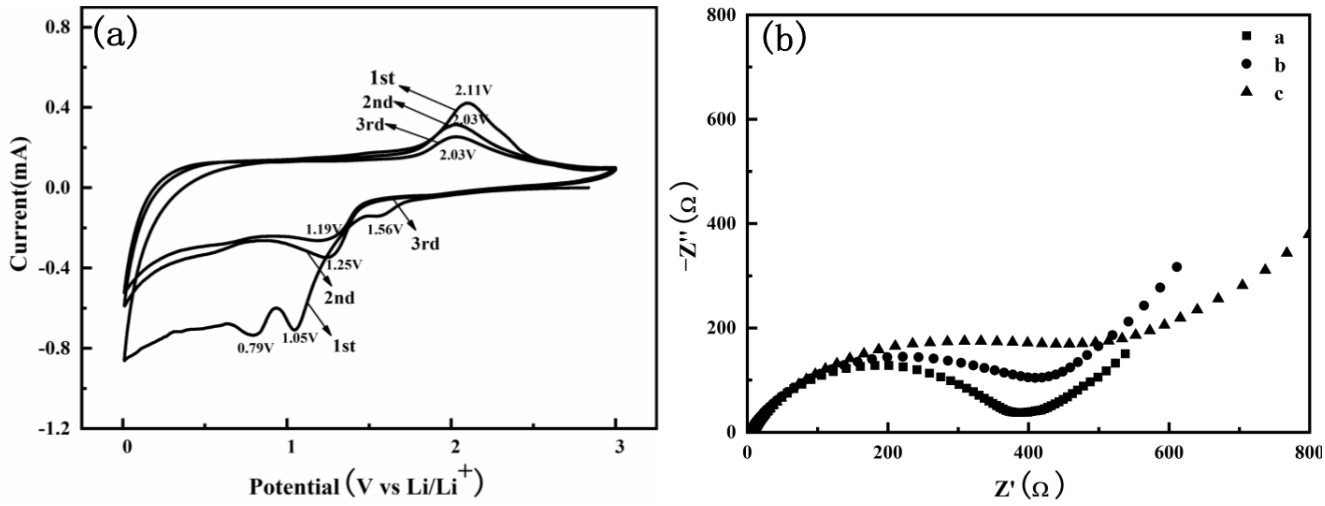

Figure 6. (a) Cyclic voltammogram of $Fe_{1-x}S$@C with 10 wt% ACET at 600 ℃ at the scanning voltage range of 0.01-3.0 V, and at a scan rate of 0.0005 $mV \cdot s^{-1}$; (b) Nyquist plots of $Fe_{1-x}S$@C with 10 wt% ACET at different calcination temperatures (a, b, and c represent the calcination temperature of 500, 600 and 700 ℃, respectively).

Figure 6(a). shows the cyclic voltammogram of the prepared material. The scanning voltage range was 0.01–3.0 V, and the scan rate was 0.0005 $mV \cdot s^{-1}$. Three reduction peaks are observed in the first cycle, in agreement with the previously reported literature [24-27], located at 1.56, 1.05, and 0.79 V, respectively. The small peak at 1.56V should be attributed to the intercalation reaction of Li, the peak at 1.05 V correspond to the conversion reaction between $Fe_{1-x}S$ and lithium ($Fe_{1-x}S + 2Li + 2e^- \rightarrow Li_2S + Fe$) [25-27]. The peak at 0.79 V could be attributed to the formation of SEI layers [17,28]. The oxidation peak at 2.11V of the first cycle corresponds to the conversion of Li_2S to $Li_{2-x}FeS_2$, the reduction peak at 1.25V of the second cycle should be attributed to the conversion of $Li_{2-x}FeS_2$ to Li_2FeS_2, and the subsequent reactions are reversible conversion reaction of $Li_{2-x}FeS_2$ and Li_2FeS_2 [25,27,29]. Onwards from the second cycle, only a significant reduction peak can be observed at 1.25 V, and the third cycle at 1.19 V. This situation indicates that there are some irreversible reactions in the first cycle. The oxidation peak shifts from 2.11 V to 2.03 V and remains by the third cycle, which implies an increase in the reversibility of the material after the second cycle. Further, the current density decreases, the peak height also becomes gentle, and the degree of coincidence between the curves of the first three weeks is not good, which indicates that the sample has undergone some irreversible reaction during the charging and discharging process in the first few weeks, resulting in irreversible capacity loss [26,30]. Figure 6(b) shows the Nyquist plots of $Fe_{1-x}S$@C (10 wt% ACET) calcined at different temperatures (the letters a, b, and c represent the calcination temperatures of 500, 600 and 700 ℃, respectively). Nyquist plots can be divided into two parts: the semi-circular portion

(charge transfer resistance, Rct) in the high frequency region represents the difficulty of charge transfer during Li^+ insertion/ extraction, and the oblique portion (Warbug resistance, Ws) in the low frequency region indicates the diffusion ability of Li^+ in the electrode reaction, respectively. The smaller Rct indicates the better kinetics of the electrochemical reaction, demonstrating the better electrochemical properties of the samples. Data fitting by using ZView software, we obtained the smallest resistance while the material calcined at 600 ℃. The resistance value of FeS@C-600 ℃ (Rct~341.9 Ω, Ws~161.1 Ω) is significantly smaller than that of the FeS@C-500 ℃ (Rct~550.9 Ω, Ws~503.1 Ω) and FeS@C-700 ℃ (Rct~401.6 Ω, Ws~401.6 Ω) samples. This conclusion is consistent with the results of constant current charge /discharge and cycle life tests, further proof the best synthesis conditions we obtained before.

4. CONCLUSION

$Fe_{1-x}S$@C materials were synthesized by a simple, convenient, and cost-effective precipitation method, using acetylene black as the carbon source. The sample prepared with 10 wt% ACET for carbon coating and calcined at 600 °C showed excellent discharge specific capacity and cycle stability, which displayed a stable high reversible capacity of 644 $mA \cdot h \cdot g^{-1}$ until the 200th cycle, and the Coulombic efficiency after stabilization was found to be close to 100%. When the sample was tested at a high rate of 500 $mA \cdot g^{-1}$, the discharge specific capacity is still satisfactory and has excellent stability, could be maintained at 470 $mA \cdot h \cdot g^{-1}$. Then the current density was reverted to 100 $mA \cdot g^{-1}$ in the 50th cycle, the discharge specific capacity of the material remained at 640 $mA \cdot h \cdot g^{-1}$ after a small attenuation. The prepared material showed significantly enhanced electrochemical performance to compared with pure $Fe_{1-x}S$, the $Fe_{1-x}S$@C materials with good electrochemical performance indicates their potential for use in LIBs.

ACKNOWLEDGMENTS
The Study was Supported by the University Scientific Research Program of Xinjiang (XJEDU2017S028) and Electrochemical Technology and Application engineering center of Xinjiang Normal University (XJNUGCZX122017B06) in China.

References

1. M. Wakihara, *Mater. Sci. Eng. R*, 33 (2001) 109.
2. E. Karden, P. Servé, B. Fricke, T. Miller, K. Snyder, *J. Power Sources*, 168 (2007) 2.
3. A. Yoshino, *Angew. Chem. Int. Edit*., 51 (2012) 5798.
4. A. Eftekhari, Z. Jian, X. Ji, *ACS Appl. Mater. Interfaces*, 9 (2016) 4404.
5. Z. Hu, Q. Liu, S. Chou, L. S., X. Dou, *Adv. Mater*., 29 (2017) 1700606.
6. L. Li, S. Peng, N. Bucher, H. Chen, N. Shen, A. Nagasubramanian, M. Srinivasan, *Nano*, 37 (2017) 81.
7. J. B. Goodenough, K. S. Park, *J. Am. Chem. Soc*., 135 (2013) 1167.
8. L. Lin, X. Xu, C. Chu, M. K. Majeed, J. Yang, *Angew. Chem. Int. Ed. Engl.*, 55 (2016) 14063.

9. V. Etacheri, R. Marom, R. Elazari, G. Salitra, D. Aurbach, *Energ. Environ. Sci.*, 4 (2011) 3243.
10. B. J. Landi, M. J. Ganter, C. D. Cress, R. A. Dileo, R. P. Raffaelle, *Energ. Environ. Sci.*, 2 (2009) 638.
11. L. Ji, Z. Lin, M. Alcoutlabi, X. Zhang, *Energ. Environ. Sci.*, 4 (2011) 2682.
12. J. M. Tarascon, M. Armand, *Nature*, 414 (2011) 359.
13. P. L. Poizot, G. S., S. Laruelle, S. Grugeon, L. Dupont, J. M. Tarascon, *Nature*, 407 (2000) 496.
14. M. H. Oh, T. Yu, S. H. Yu, B. Lim, K. T. Ko, M. G. Willinger, K. Kang, *Science*, 340 (2013) 964.
15. X. Y. Yu, H. Hu, Y. Wang, H. Chen, X. W. Lou, *Angew. Chem. Int. Ed. Engl*., 54 (2015) 7395.
16. C. Tan, H. Zhang, *Chem. Soc. Rev.*, 44 (2015) 2713.
17. X. Wei, W. Li, J. A. Shi, L. Gu, Y. Yu, *ACS Appl. Mater. Interfaces*, 7 (2015) 27804.
18. Y. Fang, Z. Chen, L. Xiao, X. Ai, Y. Cao, H. Yang, *Small*, 14 (2018) 1703116.
19. B. H. Hou, Y. Y. Wang, J. Z. Guo, Y. Zhang, Q. L. Ning, Y. Yang, X. L. Wu, *ACS Appl. Mater. Interfaces*, 10 (2018) 3581.
20. Q. Li, Q. Wei, W. Zuo, L. Huang, W. Luo, Q. An, Q. Zhang, *Chem. Sci.*, 8 (2017) 160.
21. K. Liang, K. Marcus, S. Zhang, L. Zhou, Y. Li, De Oliveira, S. T., Y. Yang, *Adv. Energy Mater.*, 7 (2017)1701309.
22. C. Zhu, Y. Wen, Van Aken, A. P., J. Maier, Y. Yu, *Adv. Funct. Mater.*, 25 (2015) 2335.
23. Q. Pan, F. Zheng, X. Ou, C. Yang, X. Xiong, Z. Tang, M. Liu, *ACS Sustainable Chem. Eng.*, 5 (2017) 4739.
24. Z. Yan, W. He, X. Zhang, X. Yang, Y. Wang, X. Zhang, G. Xu, *J. Mater. Sci. - Mater. El.*, 30 (2019) 4527.
25. Y. Xu, W. Li, F. Zhang, X. Zhang, W. Zhang, S. C. Lee, Y. Tang, *J. Mater. Chem. A*, 4 (2016) 3697.
26. F. Bu, P. Xiao, J. Chen, M. F. A. Aboud, I. Shakir, Y. Xu, *J. Mater. Chem. A*, 6 (2018) 6414.
27. C. Wang, M. Lan, Y. Zhang, H. Bian, M. F. Yuen, K. K. Ostrikov, J. Lu, *Green Chem.*, 18 (2016) 3029.
28. G. Cherkashinin, K. Nikolowski, H. Ehrenberg, S. Jacke, L. Dimesso, W. Jaegermann, *Phys. Chem. Chem. Phys.*, 14 (2012) 12321.
29. C. Wu, J. Maier, Y. Yu, *Adv. Mater*., 28 (2016) 174.
30. D. T. Tran, S. S. Zhang, *J. Mater. Chem. A,* 3 (2015) 12240.